Changes in velocity profiles in a two dimensional carotid artery geometry in response to changes in velocity waveforms and a simulated stenosis growth: A lattice Boltzmann Simulation

J Boyd, and J M Buick

***Abstract*—**It is known that low near wall velocity and shear stress are correlated to the pathogenesis and progression of atherosclerosis in the human arterial system. Obtaining accurate *in vivo* measurements of these variables is non-trivial, thus numerical modelling is often a powerful tool in the investigation of human arterial blood flow and cardiovascular diseases such as atherosclerosis. In this paper the Lattice Boltzmann Method is used to simulate blood flow in a human carotid artery geometry for three different pulsatile waveforms. A simulated stenosis growth is implemented and variations in velocity profiles across three regions of the artery are examined. Many of the flow features relating to the incidence of atherosclerosis described in the literature are observed. Significant changes in the velocity across the artery are seen in response to the simulated stenosis growth.

***Keywords*—**Lattice Boltzmann Method, carotid artery, blood flow, atherosclerosis.

I. Introduction

CARDIOVASCULAR disease is a leading cause of morbidity in the industrialised world [1], [2], particularly atherosclerotic disease. Current studies have presented a body of evidence which suggests a correlation between atherosclerosis, regions of low blood flow velocity, circulating flow, and low and oscillatory shear stress near the walls of arteries [3]–[7]. However, accurate measurements of quantities of interest are often difficult to obtain *in vivo*, thus numerical simulation becomes a valuable investigative tool.

The Lattice Boltzmann Method (LBM) [8]–[10] has been developed as an alternative method for modelling fluid flows. It uses a simplified kinetic equation to simulate fluid flows and has been successfully applied to the modelling of blood flow [11]–[19]. In this paper a simulated stenosis growth will be implemented in a two-dimensional carotid artery geometry and the change in the flow properties will be examined using the LBM. This will be done for three different pulse waveforms representing both resting and exercising heart beats.

This work was partially supported by Sigma Xi grant no. 10040015, an Australian Postgraduate Award (APA) and the Keith and Dorothy Mackay travelling scholarship.

J. Boyd and J. M. Buick (corresponding author) are with the School of Science and Technology, University of New England, Armidale, NSW, 2351 Australia, (phone: +61 2 6773 2597; fax: +61 2 6773 2844; e-mail: jbuick@une.edu.au)

II. Hemodynamical Influences Affecting the Progression of Atherosclerosis

The progression of atherosclerosis is not independent of the flow properties of the blood surrounding it. It is a geometrically focal disease [3] that occurs most frequently in the outer edges of an arterial bifurcation [3]. These regions are typically areas of disturbed flow patterns [3], [20], low velocity and low shear rates [5], [21], [22]. It is not clear why these flow factors influence the progression of atherosclerosis, but it has been postulated [4], [21], [22] that the disturbed flow zones and low shear stress lead to an increased residency time for particles near the artery wall that can promote or increase plaque progression. This is useful in predicting areas that are susceptible to atherosclerosis. For example, in the carotid artery, the asymmetrical bifurcation leads to areas of disturbed flow and low shear stress at the outer walls of the bifurcation [5], [22], this is where atherosclerosis of the carotid artery most frequently occurs [5].

It is also important to note that plaque growth does not happen suddenly but progresses smoothly in time [4], this usually results in smooth plaque formations. There is evidence to suggest that the shapes of these plaques play an important role in determining whether the plaque will rupture under the stress produced by the changed flow conditions [23], [24]. It has been suggested that irregularly shaped plaques are more likely to rupture and lead to acute coronary syndromes such as ischaemia [24], where ruptured plaque components block smaller arteries and reduce flow to important organs such as the heart or the brain. Such an occurrence can cause serious lasting injury or even death.

Being aware of these factors and how they influence plaque growth is important in the detection and treatment of atherosclerosis. In this paper, numerical modelling of the human carotid bifurcation is considered in order to provide a greater understanding of the processes involved. This may lead to new ways of detecting and treating atherosclerosis devised.

III. The Lattice Boltzmann Method

The LBM [9] has recently been developed as an alternative method for simulating a range of fluid flows. In the LBM particle distribution functions, $f_i(\mathbf{x}, t)$ at point $\mathbf{x}$

at time t,

are confined to move synchronously on a regular lattice. The distribution functions interact on the lattice such that mass and momentum are conserved while ensuring that the fluid is Galilean invariant and isotropic. Here i labels the lattice link the distribution function is on. The lattice used in this paper is the D2Q9, shown in fig. 1. The evolution of the distribution functions on the lattice is governed by the discreet Boltzmann equation [9], [25]

$$f_i(\mathbf{x}+\mathbf{e}_i, t+1) = f_i(\mathbf{x}, t) + \Omega_i(\mathbf{x}, t), \tag{1}$$

where for the D2Q9 lattice and $i = 0, \cdots, 8$, and

$$\begin{aligned} &\mathbf{e}_i = (0,0), && (i=0),\\ &\mathbf{e}_i = \left(\cos[\tfrac{\pi}{2}(i-1)], \sin[\tfrac{\pi}{2}(i-1)]\right), && (i=1,2,3,4),\\ &\mathbf{e}_i = \sqrt{2}\left(\cos[\tfrac{\pi}{2}(i-1)+\tfrac{\pi}{4}], \sin[\tfrac{\pi}{2}(i-1)+\tfrac{\pi}{4}]\right), && (i=5,6,7,8), \end{aligned} \tag{2}$$

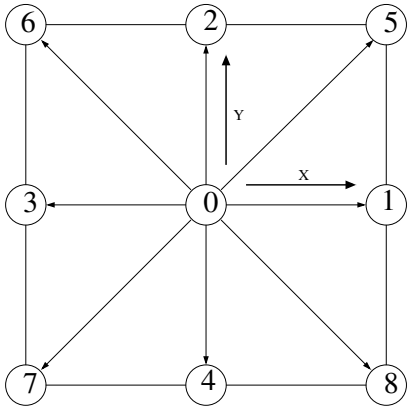

Fig. 1. D2Q9 lattice.

and Ω_i is the collision operator. The fluid density ρ and the velocity $\mathbf{u}$ can be calculated directly from the distribution functions at each node by

$$\begin{aligned} \rho &= \textstyle\sum_i f_i, \text{ and}\\ \rho\mathbf{u} &= \textstyle\sum_i f_i \mathbf{e}_i \end{aligned} \tag{3}$$

respectively. The collision operator Ω_i is given by the Bhatnagar-Gross-Krook approximation as [26],

$$\Omega_i = \frac{-1}{\tau}[f_i(\mathbf{x}, t) - f_i^{eq}(\mathbf{x}, t)], \tag{4}$$

where τ is the relaxation time and $f_i^{eq}(\mathbf{x}, t)$ is the equilibrium value of the distribution function [9], [25]. The form of the equilibrium distribution function in two dimensions is given by [25]

$$f_i^{eq}(\mathbf{x}, t) = w_i\rho[1 + 3\mathbf{e}_i \cdot \mathbf{u} + \frac{9}{2}(\mathbf{e}_i \cdot \mathbf{u})^2 - \frac{3}{2}\mathbf{u}^2], \tag{5}$$

where

$$\begin{aligned} w_0 &= \tfrac{4}{9},\\ w_i &= \tfrac{1}{9}, \text{ for } i = 1,2,3,4, \text{ and}\\ w_i &= \tfrac{1}{36}, \text{ for } i = 5,6,7,8. \end{aligned} \tag{6}$$

The relaxation time τ is related to the viscosity η by

$$\eta = \frac{(2\tau - 1)\rho}{6}. \tag{7}$$

The LBM reproduces the Navier-Stokes equation in the nearly incompressible limit and is second-order accurate in the body of the fluid [9]. A sub-grid accurate extrapolation boundary scheme [27] was used to implement the artery geometry in the model. This boundary scheme retains the second order nature of the LBM and is well suited to modelling complicated boundary geometries such as those found in the human carotid artery [14].

At the entry of the artery, a predetermined velocity profile was implemented. This boundary condition was implemented by setting the distribution functions at the entry equal to their equilibrium values, calculated from equation (5), for the desired density and velocity. The profile was applied uniformly across the width of the driving region at the base of the artery geometry, see fig. 2 a) except for a boundary layer region of approximately 1 mm over which the velocity was linearly reduced to zero. The driving region of the flow was a significant distance away from the measurement zone of the flow profiles, see fig. 2 b), it was found that small variations in the driving parameters, such as the width of the boundary layer, did not make a significant difference to the presented results.

The unknown distribution functions at an exit site $\mathbf{x}$ were found from a linear extrapolations, based on [28]

$$f_i(\mathbf{x}, t+1) = 2f_i(\mathbf{x}+\mathbf{e}_i, t+1) - f_i(\mathbf{x}+2\mathbf{e}_i, t+1). \tag{8}$$

IV. Method

Fig. 2 a) shows the geometry that was used for this simulation. In this figure the internal carotid artery (ICA), external carotid artery (ECA) and the common carotid artery (CCA) are labelled. Thirty incrementally larger stenosis growths were implemented, with every fifth increment indicated in fig. 2 b). The stenosis was placed in a region that is known to exhibit low velocity flow and be susceptible to atherosclerosis, [14], the growing stenosis was chosen to vary smoothly between increments. The final stenosis corresponds to a blockage of about 25% of the upper CCA and 37% of the lower ICA.

Three pulsatile waveforms were implemented in the simulation, see fig. 3. Waveform **A** was adapted from Holdsworth *et al* (1999) [29] and represents the blood flow velocity in a resting carotid artery. Waveform **B** is a rescaled version of waveform **A** that represents the blood flow velocity during exercise. Waveform **C** represents a more generalised pulsatile waveform that has been used in previous work by the authors [30]. It was found that two pulse periods were sufficient for any transient effects in the flow to reduce to acceptable levels.

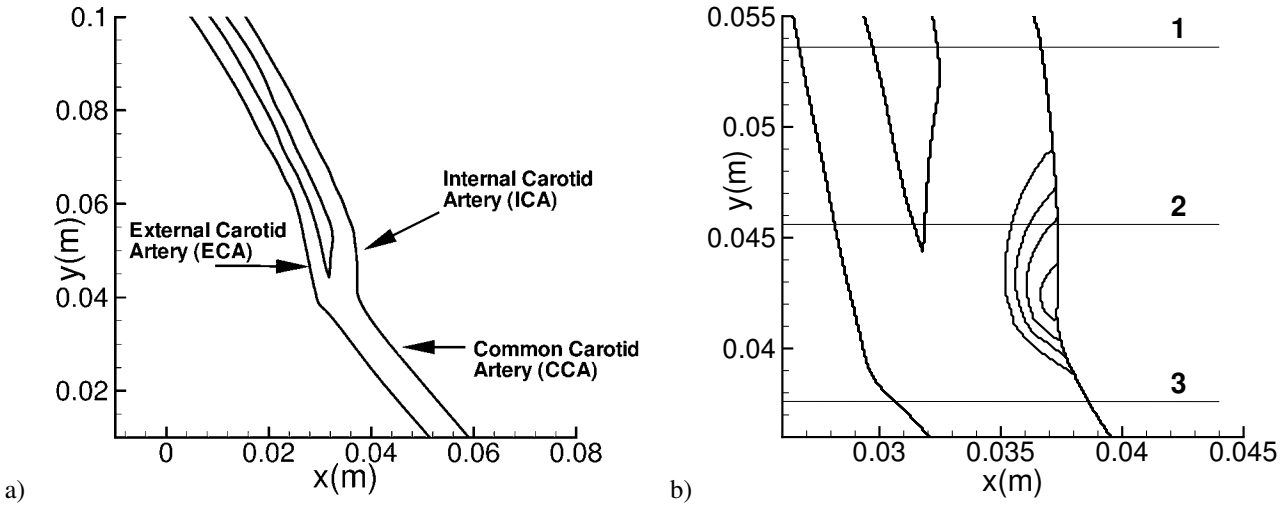

Fig. 2. a) Carotid artery geometry, b) Region of interest with incremental stenosis growths indicated. The lines **1**, **2** and **3** indicate the lines where the velocity profiles were taken.

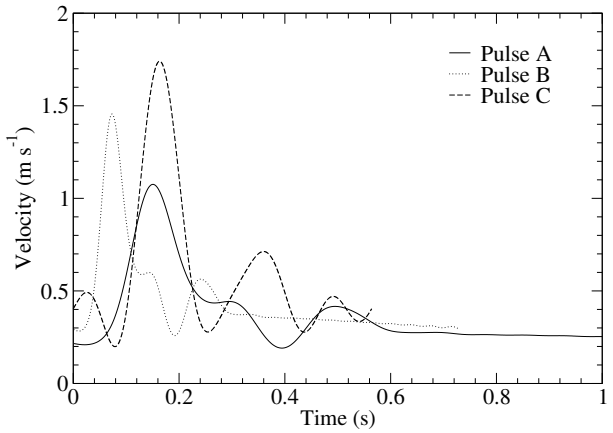

Fig. 3. Velocity waveforms **A**, **B** and **C** implemented at the base of the carotid artery geometry

A grid resolution of 12.5 grid-points per millimeter was used, and each pulse period for waveform **A** corresponded to around 4 million simulation time steps.

In order to examine the changes in the flow field due to the implemented stenosis growth, velocity profiles (VPs) were taken across the lines **1** - **3** indicated in figure 2 b). These profiles were taken at the time of peak velocity in the unstenosed geometry, which was at $t = 0.136\ s$ for waveform **A**, $t = 0.066\ s$ for waveform **B** and $t = 0.165\ s$ for waveform **C**. Figure 4 shows these VPs for stenosis increments 0, 10, 20, 25 and 30. The VPs across lines **1** and **2** shown in figures 4 a) - b), d) - e) and g) - h) show the VPs in the internal carotid artery (ICA) only, as very little flow change occurred in the external carotid artery (ECA) during the simulation.

V. Results and Discussion

A. Velocity Profiles

In general it can be seen that along lines **1** and **3**, there is very little difference between the VPs for stenosis increments 0 and 10 for all waveforms. Along line **2**, the difference between VPs for increments 0 and 10 is more noticeable, but is still the smallest difference between all stenosis increments. It is noted that the boundary of stenosis increment 10 occurs just before an interface between higher velocity flow in the central region of the CCA and a region of lower velocity flow near the right hand wall [14]. The largest changes in the velocity flow field (VFF) occur just after the stenosis boundary grows into the higher velocity central flow. Lines **1** and **3** represent flows in the upper and lower regions of the carotid artery, whereas the last portion of line 2 resides inside a region of low velocity flow near the site of the stenosis growth. Thus it can be seen the simulated stenosis growth only has a local impact on the VFF whilst its boundaries are still in this initial region of low velocity flow close to the wall.

Along each of the lines **1** - **3** the maximum velocity reached increases from waveform **A** - **C**. Along lines **1** and **2** the maximum velocity reached increases with each incremental stenosis growth with a final maximum being obtained when increment 30 was implemented. Across line **3**, although the maximum velocity attained increases from waveform **A** - **C**, this maximum is not attained with the largest stenosis incremented. It is observed from figures 4 g) - i) that across line **3** the maximum velocity attained is in the unstenosed artery. A significant change in the position of the maximum velocity was also observed along line **3**. The maximum velocity moved away from the stenosed wall as the size of the stenosis increased.

The overall shape of the VPs across lines **1** and **2** remain similar between waveforms. The VPs across line **1** for wave-

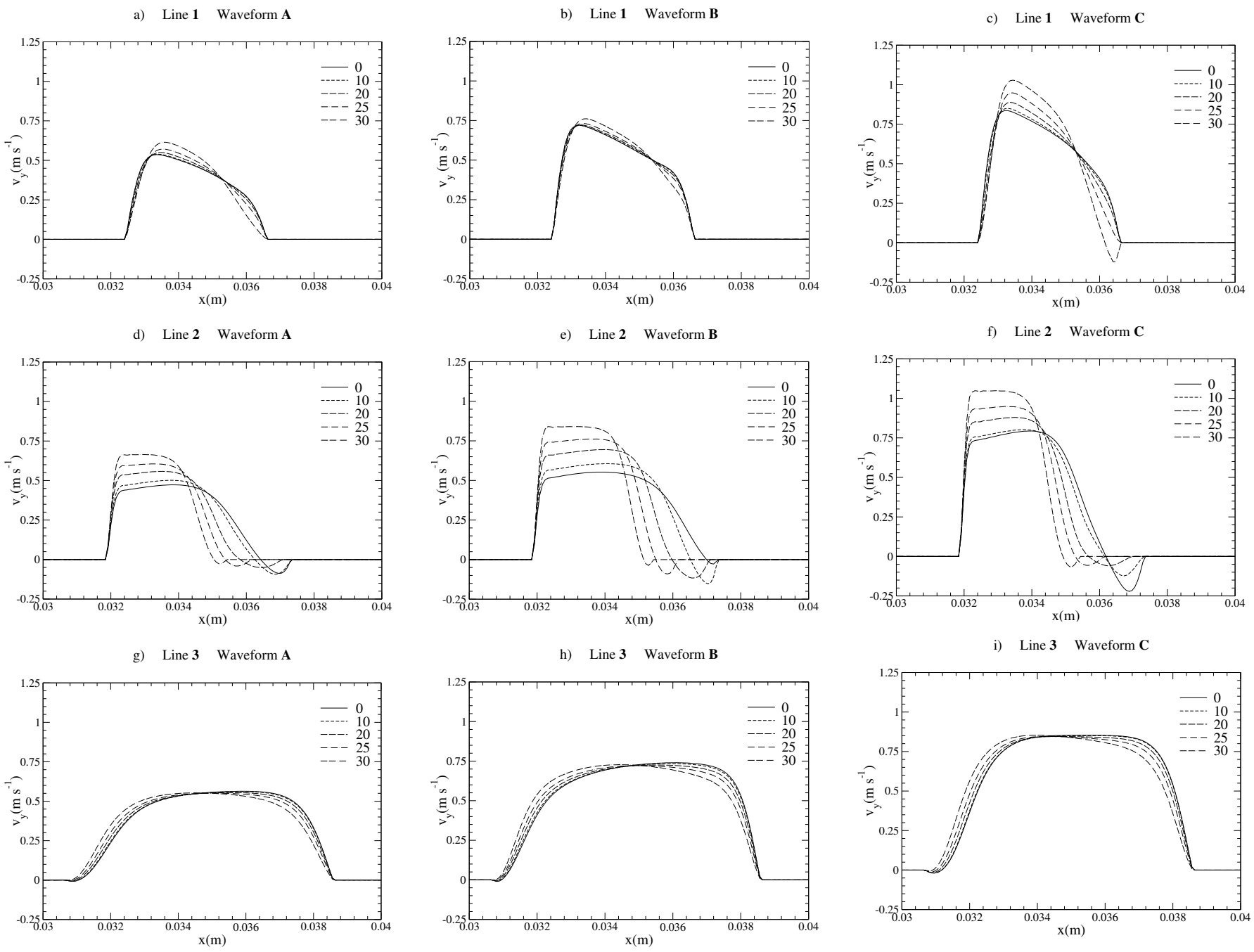

Fig. 4. Velocity profiles across lines **1** - **3** for waveforms **A** - **C**

forms **A** and **B** retain the same general shape, although for waveform **B** the velocity is higher and the region of high velocity flow extends across a greater portion of the ECA. There is also much less relative difference between the VPs for the first four stenosis increments, with the largest velocity difference occurring between increments 25 and 30.

The VP across line **1** for waveform **C** retains the same shape for the VPs for most stenosis increments. However for increment 30, a large negative flow, reaching a maximum magnitude of 0.12 m s^{-1}, occurs near the right hand wall, which does not happen for waveforms **A** and **B**. This could be an artifact of the qualitatively different shape of waveform **C** compared to those of **A** and **B**. But if this negative velocity is a result of the higher peak velocity of the waveform, this would indicate that after a critical velocity is reached, a region of circulating flow may occur immediately after the stenosis, a development which may lead to interesting shear stress effects on the wall of the stenosis in that area.

The VP shapes across line **2** also share similarities between waveforms. In all cases, the stenosis encroaches upon line **2** which leads to a narrowing of the VPs. This narrowing leads to a higher overall velocity in this region of the artery. The differences in the VPs across line **2** also show the greatest variation over the incremental stenosis growths.

The VPs across line **2** consistently exhibit areas of negative flow near the right wall of the artery. For waveforms **A** and **B** this negative velocity increases between increments 0 and 10 and decreases thereafter, whereas for waveform **C** it steadily decreases between increments 0 - 25 and increases slightly for increment 30.

The portion of **2** which exhibits negative velocity flow is in a large region of overall low velocity flow [14]. Between increments 20 - 30 the extent of this region decreases significantly, thus reducing the negative flow. However, a large region of low velocity flow, and presumably regions of negative flow, still persist immediately upstream of the growing stenosis.

Across line **3** the VP shapes are also similar for all waveforms. The VPs highest point on the VP shape moves leftwards towards the central region of the artery in response to stenosis growth. This indicate an increase in flow towards the bifurcation and also perhaps into the ECA. The near wall shear stress around the bifurcation increases in response to stenosis growth [14], probably as a result of this change in the VP shape. Although the peak velocity along line **3** reduces in response to stenosis growth, this reduction is only small, with a maximum decrease of 0.01 m s^{-1} for waveform **C**. This decrease is due to the position of the stenoses on the right hand wall of the CCA.

B. Rotational Flow

Atherosclerosis occurs in regions of disturbed flow [3], [20], including areas where flow circulation is present. Such flow may occur in regions where there is a large velocity gradient in a small area. From figure 4 it is observed that areas satisfying these condition exist on the outer wall of the ICA. These areas are characterized by an area of low velocity near the edge of the artery surrounded by the higher velocity central flow. These regions are slowly rotating, as indicated by the relatively small velocities in these regions. This suggests that if a particle in the blood was trapped in the region, it would probably stay in that region for some time. The lowest velocity flow also occurs nearest the walls of the artery. This lends insight into the prevalence of atherosclerosis on the outer walls near the bifurcation of the carotid artery [5].

An important question to ask at this point is whether these regions of flow circulation are preserved during progressive plaque buildup. The results in figure 4 suggest that this region does persist, due to the observed negative flow velocities across line **2** near the stenosis for all waveforms. Previously published results [14] also suggest this for waveform **A**.

Figures 5 a) - f) show vector maps of the VFF for the stenosis growth in the region near the outer wall of the ICA with waveform **A** implemented for stenosis increments of 5, 10, 15, 20, 25 and 30 respectively. The vectors are of uniform length, the fluid direction is indicated by the arrows and the magnitude by the colour map. We note that in the simulation the artery wall is smooth. The step like wall in figure 5 is an artifact of the plotting routine. It can be seen from figures 5 a) - f) that the area of circulation persists during the stenosis growth. The disturbed area of flow remains upstream of the growing stenosis, and stays close to the wall. This corresponds to the behaviour seen in figures 4 d) - f) and in previous literature results [14].

The overall velocity distributions within the rotational flow also remain similar during the stenosis growth. The velocities near the wall increase during the stenosis growth, but still remain low in comparison with the central fluid flow. This would suggest that the stenosis growth preserves a region of low velocity, rotational flow. Such regions would have higher particle residency times for particles which get caught in them.

We recall from figures 4 d) - f) that waveforms **A** - **C**, correspond to increasingly higher peak waveform velocities. The areas of negative velocity in figures 5 a) - f) increase in magnitude with increasing waveform peak velocity. This would suggest that while circulation is present for each waveform, the rate of rotation increases, so that particle residency time would probably be reduced in the higher velocity waveforms that correspond to exercising heartbeats.

VI. Conclusion

A number of interesting effects were observed. Areas of low velocity and circulating flow were found in regions of the unstenosed artery which are typically susceptible to atherosclerosis. This was observed for all waveforms. In particular for waveform **A** it was observed that these areas of low velocity rotational flow were preserved during the simulated stenosis growth and remained adjacent to the stenosis growth.

Regions of rapid velocity change corresponding to regions of high shear were also observed near the stenosis wall. The change in velocity was greater for waveform **C**, indicating that the narrowing of the artery created higher shears near the wall of the stenosis. The may have implications for the process by which stenosis rupture.

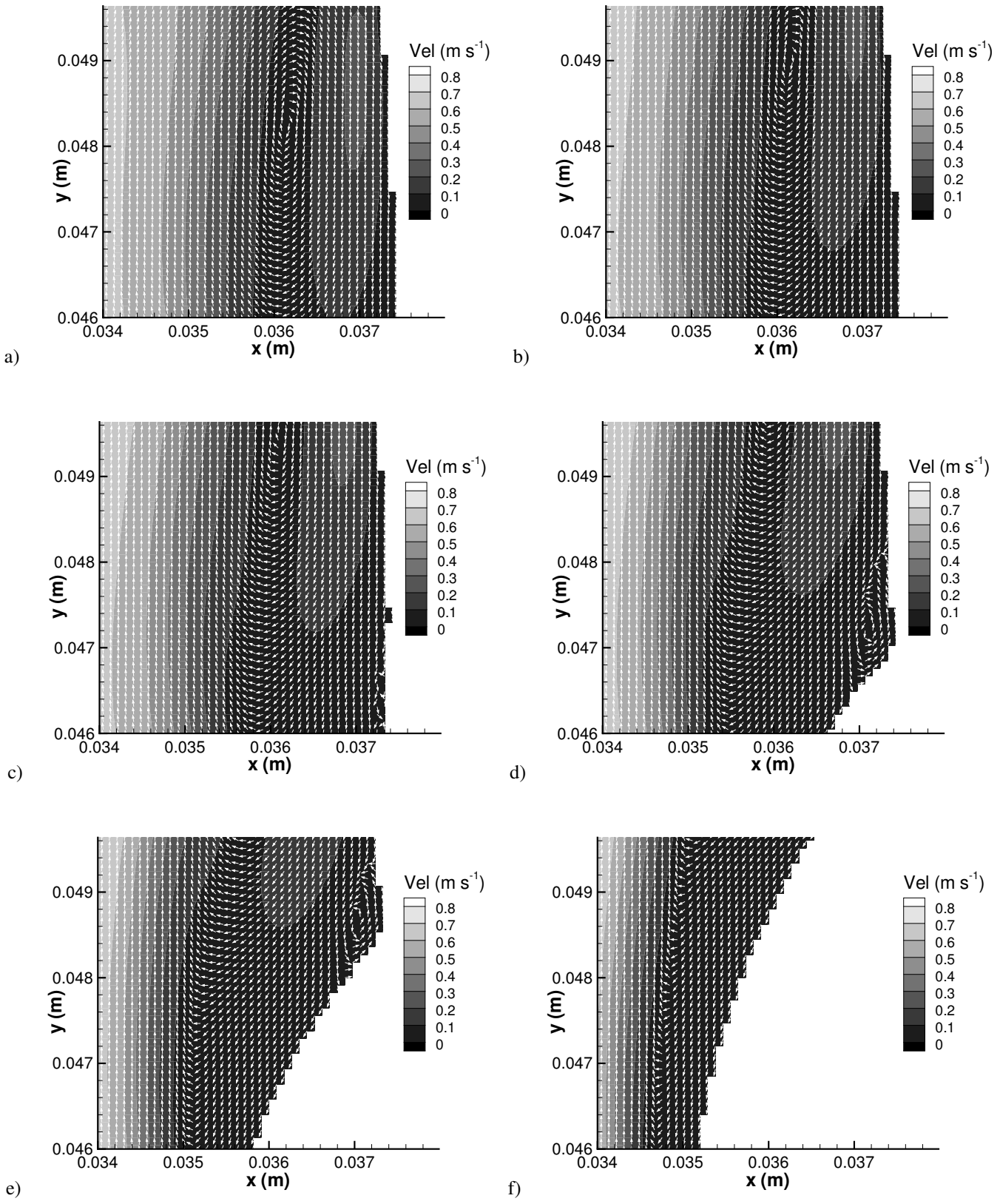

Fig. 5. Movement of rotational flow at $t = 0.136$ in response to stenosis growth on the outer wall of the ICA for waveform **A** for stenosis increments of a) 5, b) 10, c) 15, d) 20, e) 25 and f) 30.

Many of the arterial flow properties that are associated with atherosclerotic progression have been observed, indicating the suitability of the LBM for this application.

REFERENCES

[1] C. J. L. Murray and A. D. Lopez, *The global burden of disease: a comprehensive assessment of mortality and disability from diseases, injuries, and risk factors in 1990 and projected to 2020,* Harvard school of public health MA 1996

[2] C. G. Caro, "Vascular fluid dynamics and vascular biology and disease," *Math. Methods Appl. Sci* 24, 2001, pp. 1311–1324.

[3] A. M. Malek, S. L. Alper and S. Izumo, "Hemodynamic Shear Stress and Its Role in Atherosclerosis," *J. Am. Med. Assoc.* 282, 1999, pp. 2035–2042.

[4] T. Asakura and T. Karino, Flow Patterns and Spatial "Distribution of Atherosclerotic Lesions in Human Coronary Arteries," *Circ. Res.* 66, 1990, pp. 1045–1066.

[5] A. Gnasso, C. Irace, C. Carallo, M. S. De Franceschi, C. Motti, P. L. Mattioli and A. Pujia, "In Vivo Association Between Low Wall Shear Stress and Plaque in Subjects With Asymmetrical Carotid Atherosclerosis," *Stroke* 28, 1997, pp. 993–998.

[6] D. N. Ku, D. P. Giddens, C. K. Zarins and S. Glagov, "Pulsatile Flow and Atherosclerosis in the Human Carotid Bifurcation: Positive Correlation between Plaque Location and Low and Oscillating Shear Stress," *Arteriosclerosis* 5(3), 1985, pp. 293–302.

[7] D. C. Chappell, S. E. Varner, R. M. Nerem, R. M. Medford and R. W. Alexander, "Oscillatory Shear Stress Stimulates Adhesion Molecule Expression in Cultured Human Endothelium," *Circ. Res.* 82, 1998, pp. 532–539.

[8] D. A. Wolf-Gladrow, *Lattice-Gas Cellular Automata and Lattice Boltzmann Models, An introduction,* Springer 2000

[9] S. Chen and G. D. Doolen, "Lattice Boltzmann method for fluid flows," *Ann. Rev. Fluid Mech.* 30, 1998, pp. 329–364.

[10] S. Succi, *The Lattice Boltzmann Equation for Fluid Dynamics and Beyond,* Oxford University Press 2001

[11] M. Krafczyk, M. Cerrolaza, M. Schulz and E. Rank, "Analysis of 3D transient blood flow passing through and artificial aortic valve by Lattice-Boltzmann methods," *J. Biomech.* 31, 1998, pp. 453–462.

[12] A. M. Artoli, A. G. Hoekstra and P. M. A. Sloot, "3D Pulsatile Flow With the Lattice Boltzmann BGK Method," *Int. J. Mod. Phys. C* 13(8), 2002, pp. 1119–1134.

[13] A. M. Artoli, A. G. Hoekstra and P. M. A. Sloot, "Simulation of a systolic cycle in a realistic artery with the Lattice Boltzmann BGK method," *Int. J. Mod. Phys. B* 17(1-2), 2003, pp. 95–98.

[14] J. Boyd, J. M. Buick, J. A. Cosgrove and P. Stansell, "Application of the lattice Boltzmann model to simulated stenosis growth in a two-dimensional carotid artery," *Phys. Med. Biol.* 50, 2005, pp. 4783–4796.

[15] R. Ouared and B. Chopard, "Lattice Boltzmann Simulations of Blood flow: Non-Newtonian Rheology and Clotting Processes," *J. Stat. Phys.* 121(1/2), 2005, pp. 209–221.

[16] A. M. Artoli, A. G. Hoekstra and P. M. A. Sloot, "Mesoscopic simulations of systolic flow in the human abdominal aorta," *J. Biomech.* 39(5), 2006, pp. 873–884

[17] J. Boyd and J. M. Buick, "Comparison of Newtonian and non-Newtonian flows in a two-dimensional carotid artery model using the lattice Boltzmann method," *Phys. Med. Biol.* 52(20), 2007, pp. 6215–6228.

[18] H. Fang, Z. Wang, Z. Lin and M. Liu, "Lattice Boltzmann method for simulating the viscous flow in large distensible blood vessels," *Phys. Rev. E* (65), 2002, pp. 051925:1–11.

[19] H. B. Li, H. Fang, Z. Lin, S. X. Xu and S. Chen, "Lattice Boltzmann simulation on particle suspensions in a two-dimensional symmetric stenotic artery," *Phys. Rev. E* 69(33), 2004, pp. 031919

[20] A. Quarteroni, M. Tuveri and A. Veneziani, "Computational vascular fluid dynamics: problems, models and methods," *Comput. Visual. Sci*, 2, 2000, pp. 163–197

[21] C. G. Caro, J. M. Fitz-Gerald and R. C. Schroter, "Atheroma and arterial wall shear, Observation, correlation and proposal of a shear dependant mass transfer mechanism for atherogenesis," *P. Roy. Soc. Lond. B. Bio.*, 177, 1971, pp. 109–159

[22] C. K. Zarins, D. P, Giddens, B. K. Bharadvaj, V. S. Sottiurai, R. F. Mabon and S. Glagov, "Carotid Bifurcation Atherosclerosis, Quantitative Correlation of Plaque Localisation with Flow Velocity Profiles and Wall Shear Stress,", *Circ. Res.*, 53, 1983, pp. 502–514

[23] P. D. Richardson, M. J. Davies and G. V. R. Born, "Influence of plaque configuration and stress distribution on fissuring of coronary atherosclerotic plaques," *The Lancet* 21, 1989, pp. 941–944.

[24] P. M. Rothwell, R. Villagra, R. Gibson, R. C. J. M. Donders and C. P. Warlow, "Evidence of a chronic systemic cause of instability of atherosclerotic plaques," *The Lancet* 355, 2000, pp. 19–24

[25] Y. H. Qian, D. d'Humieres and P. Lallemand, "Lattice BGK models for Navier-Stokes equation," *Europhys. Lett.* 17(6), 1992, pp. 479–484.

[26] P. L. Bhatnagar, E. P. Gross and M. Krook, "A model for collision processes in gases. I: small amplitude processes in charged and neutral one-component system," *Phys. Rev.* 94, 1954, pp 511–525.

[27] Z. Guo, C. Zheng and B. Shi, "An extrapolation method for boundary conditions in lattice Boltzmann method," *Phys. Fluids* 14(6), 2002, pp. 2007–2010

[28] M. Neal, *A study of the brass instrument lip reed mechanism using artificial lips and lattice Boltzmann flow simulation*, PhD Thesis, The University of Edinburgh, 2002

[29] D. W. Holdsworth, C. J. D. Norley, R. Frayne, D. A. Steinman and B. K. Rutt, "Characterisation of common carotid artery blood-flow waveforms in normal human subjects," *Physiol. Meas.* 20, 1999, pp. 219–240

[30] J. Boyd, J. M. Buick, J. A. Cosgrove and P. Stansell, "Application of the lattice Boltzmann method to arterial flow simulation: Investigation of boundary conditions for complex arterial geometries," *Australasian Physical and Engineering Sciences in Medicine*, 27(4), 2004, pp. 147–152